Fast two-layer two-photon imaging of neuronal cell populations using an electrically tunable lens

Grewe, B F ; Voigt, F F ; van 't Hoff, M ; Helmchen, F

DOI: https://doi.org/10.1364/BOE.2.002035

Fast two-layer two-photon imaging of neuronal cell populations using an electrically tunable lens

Benjamin F. Grewe,[1,3] Fabian F. Voigt,[1,3] and Marcel van 't Hoff,[1] and Fritjof Helmchen[1,*]

[1]*Department of Neurophysiology, Brain Research Institute, University of Zurich, Winterthurerstrasse 190, CH-8057 Zürich, Switzerland*
[3]*Equal contribution*
**helmchen@hifo.uzh.ch*

Abstract: Functional two-photon Ca^{2+}-imaging is a versatile tool to study the dynamics of neuronal populations in brain slices and living animals. However, population imaging is typically restricted to a single two-dimensional image plane. By introducing an electrically tunable lens into the excitation path of a two-photon microscope we were able to realize fast axial focus shifts within 15 ms. The maximum axial scan range was 0.7 mm employing a 40x NA0.8 water immersion objective, plenty for typically required ranges of 0.2–0.3 mm. By combining the axial scanning method with 2D acousto-optic frame scanning and random-access scanning, we measured neuronal population activity of about 40 neurons across two imaging planes separated by 40 μm and achieved scan rates up to 20–30 Hz. The method presented is easily applicable and allows upgrading of existing two-photon microscopes for fast 3D scanning.

OCIS codes: (180.6900) Three-dimensional microscopy; (180.4315) Nonlinear microscopy; (170.0180) Microscopy; (170.2520) Fluorescence microscopy (180.2520) Fluorescence microscopy

References and links

1. F. Helmchen and W. Denk, "Deep tissue two-photon microscopy," Nat. Methods **2**(12), 932–940 (2005).
2. B. F. Grewe and F. Helmchen, "Optical probing of neuronal ensemble activity," Curr. Opin. Neurobiol. **19**(5), 520–529 (2009).
3. J. N. Kerr and W. Denk, "Imaging in vivo: watching the brain in action," Nat. Rev. Neurosci. **9**(3), 195–205 (2008).
4. W. Göbel, B. M. Kampa, and F. Helmchen, "Imaging cellular network dynamics in three dimensions using fast 3D laser scanning," Nat. Methods **4**(1), 73–79 (2007).
5. B. F. Grewe, D. Langer, H. Kasper, B. M. Kampa, and F. Helmchen, "High-speed in vivo calcium imaging reveals neuronal network activity with near-millisecond precision," Nat. Methods **7**(5), 399–405 (2010).
6. W. Göbel and F. Helmchen, "New angles on neuronal dendrites in vivo," J. Neurophysiol. **98**(6), 3770–3779 (2007).
7. A. M. Kerlin, M. L. Andermann, V. K. Berezovskii, and R. C. Reid, "Broadly tuned response properties of diverse inhibitory neuron subtypes in mouse visual cortex," Neuron **67**(5), 858–871 (2010).
8. E. Botcherby, C. Smith, M. Booth, R. Juskaitis, and T. Wilson, "Arbitrary-scan imaging for two-photon microscopy," Proc. SPIE **7569**(756917), 756917, 756917-8 (2010).
9. E. J. Botcherby, R. Juskaitis, M. J. Booth, and T. Wilson, "Aberration-free optical refocusing in high numerical aperture microscopy," Opt. Lett. **32**(14), 2007–2009 (2007).
10. E. J. Botcherby, R. Juskaitis, M. J. Booth, and T. Wilson, "An optical technique for remote focusing in microscopy," Opt. Commun. **281**(4), 880–887 (2008).
11. E. E. Hoover, M. D. Young, E. V. Chandler, A. Luo, J. J. Field, K. E. Sheetz, A. W. Sylvester, and J. A. Squier, "Remote focusing for programmable multi-layer differential multiphoton microscopy," Biomed. Opt. Express **2**(1), 113–122 (2011).
12. P. A. Kirkby, K. M. Srinivas Nadella, and R. A. Silver, "A compact Acousto-Optic Lens for 2D and 3D femtosecond based 2-photon microscopy," Opt. Express **18**(13), 13720–13745 (2010).
13. G. Duemani Reddy, K. Kelleher, R. Fink, and P. Saggau, "Three-dimensional random access multiphoton microscopy for functional imaging of neuronal activity," Nat. Neurosci. **11**(6), 713–720 (2008).

#144186 - $15.00 USD Received 28 Mar 2011; revised 10 Jun 2011; accepted 10 Jun 2011; published 23 Jun 2011

14. D. Vučinić and T. J. Sejnowski, "A compact multiphoton 3D imaging system for recording fast neuronal activity," PLoS ONE **2**(8), e699 (2007).
15. W. Amir, R. Carriles, E. E. Hoover, T. A. Planchon, C. G. Durfee, and J. A. Squier, "Simultaneous imaging of multiple focal planes using a two-photon scanning microscope," Opt. Lett. **32**(12), 1731–1733 (2007).
16. H. Oku, K. Hashimoto, and M. Ishikawa, "Variable-focus lens with 1-kHz bandwidth," Opt. Express **12**(10), 2138–2149 (2004).
17. B. H. W. Hendricks, S. Kuiper, M. A. J. Van As, C. A. Renders, and T. W. Tukker, "Electrowetting-based variable-focus lens for miniature systems," Opt. Rev. **12**(3), 255–259 (2005).
18. B. Berge and J. Peseux, "Variable focal lens controlled by an external voltage: An application of electrowetting," Eur. Phys. J. E **3**(2), 159–163 (2000).
19. D. Koyama, R. Isago, and K. Nakamura, "Compact, high-speed variable-focus liquid lens using acoustic radiation force," Opt. Express **18**(24), 25158–25169 (2010).
20. S. Liu and H. Hua, "Extended depth-of-field microscopic imaging with a variable focus microscope objective," Opt. Express **19**(1), 353–362 (2011).
21. K. S. Lee, P. Vanderwall, and J. P. Rolland, "Two-photon microscopy with dynamic focusing objective using a liquid lens," Proc. SPIE **7569**, 756923, 756923-7 (2010).
22. P. S. Tsai, B. Migliori, K. Campbell, T. N. Kim, K. Kam, A. Groisman, and D. Kleinfeld, "Spherical aberration correction in nonlinear microscopy and optical ablation using a transparent deformable membrane," Appl. Phys. Lett. **91**(19), 191102 (2007).
23. H. Gross, F. Blechinger, and B. Achtner, *Handbook of Optical Systems*, 1st ed. (Wiley-VCH, 2008), Vol. 4.
24. A. Katsuyuki, "Embodiment 1," Japanese Patent 8–292374 (Nov. 5, 1996).
25. W. S. Rasband and J. Image, U. S. National Institutes of Health, Bethesda, Maryland, USA, 1997–2009, http://rsb.info.nih.gov/ij/.
26. C. Stosiek, O. Garaschuk, K. Holthoff, and A. Konnerth, "In vivo two-photon calcium imaging of neuronal networks," Proc. Natl. Acad. Sci. U.S.A. **100**(12), 7319–7324 (2003).
27. A. Nimmerjahn, F. Kirchhoff, J. N. Kerr, and F. Helmchen, "Sulforhodamine 101 as a specific marker of astroglia in the neocortex in vivo," Nat. Methods **1**(1), 31–37 (2004).
28. A. Cheng, J. T. Gonçalves, P. Golshani, K. Arisaka, and C. Portera-Cailliau, "Simultaneous two-photon calcium imaging at different depths with spatiotemporal multiplexing," Nat. Methods **8**(2), 139–142 (2011).
29. M. Blum and A. G. Optotune, Ueberlandstrasse 129, Dubendorf, Switzerland (personal communication, 2011).

1. Introduction

Two-photon calcium imaging allows recording of neuronal activity in the intact brain down to depths of several hundred micrometers [1–3]. Due to the nonlinear excitation with femtosecond near-infrared laser pulses, fluorescence is exclusively generated at the laser focus. While scanning the focal excitation spot perpendicular to the optical axis provides a 2D image, shifting the excitation spot along the optical axis enables 3D imaging. For probing the activity of extended neuronal populations in the intact brain, 3D imaging is especially helpful, as the number of cells that can be recorded strongly increases with volume [4]. However, single-trial recordings of neuronal network activity in 3D require fast imaging techniques to obtain a complete picture of local Ca^{2+}-dynamics with high temporal resolution [4]. The ideal Ca^{2+}-imaging method would allow three-dimensional measurements throughout hundreds of micrometers of tissue to sample large neuronal populations within a few milliseconds. Clearly, adding a third scan dimension exacerbates the challenge to record from neuronal populations with high sampling rates.

While new 2D scan techniques for in vivo population imaging achieve sampling rates from ten up to several hundred Hertz [5], typical maximum 3D scanning rates are lower, mostly due to the limit set by the inertia of the moving objective. The combination of galvanometric x/y-scan mirrors with a piezoelectric z-focusing device attached to the microscope objective was demonstrated to allow custom 3D frame and line scan modes to record calcium signals of several hundred neurons in vivo with sampling rates up to 10 Hz [6,7]. The inertia of the moving objective clearly restricts the z-scanning speed of these approaches. Additionally, the oscillation of the objective may render stable simultaneous electrical recordings difficult. To overcome these limitations, remote focusing schemes have been proposed, which separate focal shift and excitation duties of the microscope objective by adding an intermediate imaging stage [8–10]. Recently, an array of such remote focusing systems was shown to allow multi-layer imaging in combination with spatiotemporal multiplexing [11]. This technique uses the sequential timing of laser pulses that can be focused at different focal depths and

#144186 - $15.00 USD Received 28 Mar 2011; revised 10 Jun 2011; accepted 10 Jun 2011; published 23 Jun 2011

assigns the detected fluorescence signal to the correct plane of origin accordingly. Another alternative to inertia-limited z-scanners are special arrangements of 2-4 acousto-optical deflectors (AODs) acting as acousto-optical lenses, enabling high-speed imaging in 3D [12–14]. The basic idea of these approaches is to employ chirped acoustic waves traveling through the AODs to control beam divergence in addition to deflection angle, resulting in a movement of the excitation spot along the z-axis.

Further approaches to realize 3D scanning combine tunable optical components with standard microscope optics, including the use of deformable mirrors for axial scanning [15] and the development of high-speed tunable lenses for fast focusing [16]. The technology of tunable lenses has progressed rapidly during the recent years; different lens types have been proposed based on electrowetting [17,18], piezo-hydraulic actuation [16], or acoustic radiation force [19]. Successful integration of tunable lenses into microscopes enables a wide variety of applications, including extended-depth-of-field imaging [20], axial focusing in two-photon microscopy [21] and the compensation of spherical aberration induced by refractive index mismatch in tissue [22].

Here, we describe how to upgrade a conventional 2D two-photon microscope for fast three dimensional imaging by using a commercially available electrically tunable lens (ETL) as an axial scanning device. We characterize the optical performance of our adapted two-photon microscope system and demonstrate its feasibility for 3D in vivo calcium imaging of neuronal cell populations. Using an offset lens of negative focal length and a standard water-dipping microscope objective we were able to shift the focal spot along the optical axis with a range of up to 700 μm. We characterized the dynamical properties of the ETL and optimized the driving signal to allow axial relocation of the excitation spot between focal planes within 15 milliseconds. Incorporation of the ETL focusing system into our custom AOD-based two-photon microscope enabled fast two-layer frame-scanning and random-access scanning on a preselected set of 40 cells spread across two planes at different focal depths with sampling rates of up to 20-30 Hz. Our new method with the electrically tunable lens and the concave offset lens as key components is straightforward, cost-efficient, easily installed and can be used to render standard two-photon microscopes suitable for fast 3D imaging.

2. Experimental setup and optical performance

2.1. Microscope setup

While most experiments were performed using a custom built two-photon microscope that employs two acousto-optic laser scanners [5], we also tested the ETL in combination with a standard two-photon microscope equipped with galvanometric scan mirrors [4] for precise resolution measurements. All experiments were done using a 40x water-dipping microscope objective (Olympus LUMPlanFL, 40xW, NA 0.8).

2.2. Axial scanning with an electrically tunable lens

To generate a divergent or convergent laser beam at the rear aperture of the microscope objective we combined a convex ETL (EL-C-10-30-VIS-LD, tuned to a range of +50 to +200 mm focal length 10 mm clear aperture, Optotune AG, Switzerland) with different concave offset lenses (Fig. 1a, upper panel). The ETL consists of a flexible spherical membrane that changes its radius depending on the pressure exerted on its outer zone by a voice-coil actuated ring. The active surface is environmentally sealed between two cover glasses (Fig. 1a). ETLs are well suited for microscopic applications, because they allow fast changes of the focal length by varying the applied current, while maintaining a large aperture size. Both ETL and offset lens were mounted in a custom-built holder to which the microscope objective was attached (Fig. 1b). Axial distances were 2.4 mm between the ETL and the plane surface of the offset lens and 4.5-5 mm between the vertex of the concave surface of the offset lens (OL) and the mounting shoulder of the microscope objective. The

#144186 - $15.00 USD Received 28 Mar 2011; revised 10 Jun 2011; accepted 10 Jun 2011; published 23 Jun 2011

magnetic actuator of the ETL was controlled by a custom current controller, which delivered a stable current output from 0 to 200 mA at a maximum of 5 V. Alternatively, the ETL can be driven by a standard laser diode current driver (LD1255P, Thorlabs). To avoid vignetting, the lens assembly was positioned as close as possible to the objective's rear stop. For focusing along positive and negative directions of the optical axis we tested the ETL in combination with different concave OLs of −48 mm (Edmund Optics, NT47-907), −75 mm (Thorlabs, LC4413) and −100 mm (Thorlabs, LC4432) focal length (Fig. 1c). Axial focus shifts were measured by refocusing small 0.5 µm fluorescent beads (Fluoresbrite, Polysciences Inc.) using a motorized z-stage with a precise rotation encoder (PMT160, Feinmess, Germany). To minimize optical aberrations of the laser beam we finally chose the f = −100 mm concave OL for further studies. This combination allowed a suitable axial shift of the focus position from −115 µm (0 mA) to + 600 µm (200 mA). Positive axial focus shifts refer to a decrease in working distance of the objective and vice versa. To further demonstrate the axial scanning ability of this lens combination we imaged pollen grains without and with the ETL/OL lens assembly inserted at different axial positions while relocating the focus with the z-stage (Fig. 1 d,e). While the ETL would allow an even larger focal range (possible ETL current from 0 to 400 mA), our axial scanning range was electronically limited to about 700 µm, which however is an ample range for most in vivo two-photon imaging applications. In our configuration both laser excitation beam and the fluorescence signal travel through the ETL. In order to optimize the fluorescence signal collection efficiency we chose a VIS-coating

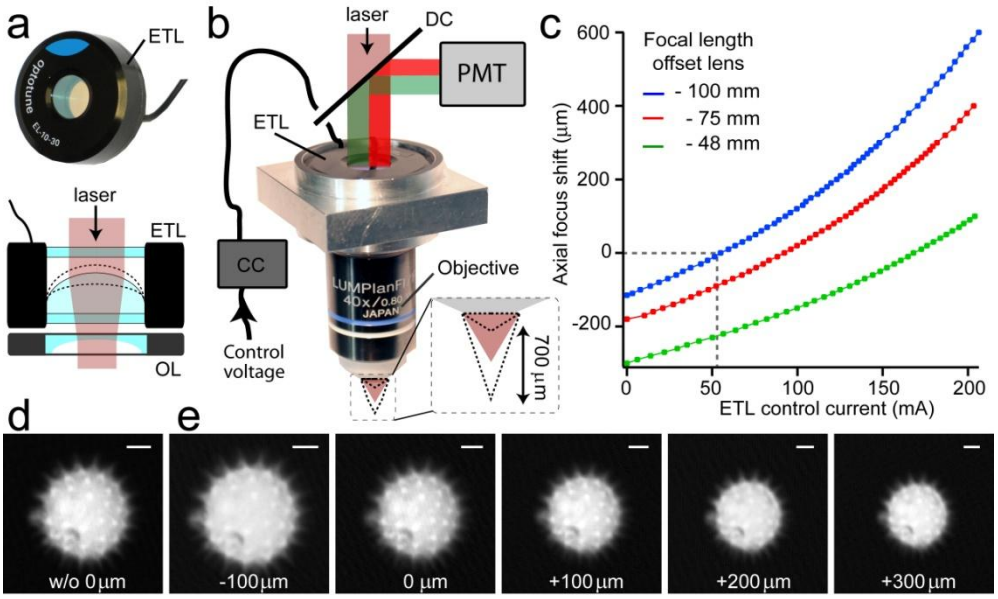

Fig. 1. Optical setup and focusing properties of the electrically tunable lens. (a) Upper panel: Electrically tunable lens (ETL). Lower panel: lens assembly consisting of the ETL and the offset lens (OL). (b) Microscope adaptor to mount and align the ETL/OL assembly with respect to the microscope objective and excitation/detection pathways. DC dichroic beam splitter, PMT photomultiplier, CC current control driver. (c) Electrical focusing behavior of the ETL/OL system shown in (b) for three different plano-concave offset lenses (focal lengths: −100 mm/blue, −75 mm/red, −48 mm/green) in combination with the 40x objective. The axial focus shift was measured by refocusing small fluorescent beads using the motorized z-stage of the microscope. (d) Two-photon image (taken with the AOD microscope) of a pollen grain imaged without the ETL/OL assembly inserted. (e) The same pollen grain imaged through the ETL/OL/Objective assembly at different axial focus shifts. The pollen grain was refocused to the imaging plane in (d) using a motorized z-stage. Note the change in magnification or field-of-view size. Scale bars, 5 µm.

#144186 - $15.00 USD Received 28 Mar 2011; revised 10 Jun 2011; accepted 10 Jun 2011; published 23 Jun 2011

option for both ETL cover glasses (transmission >90% VIS, >70% NIR). The resulting total transmission of the lens combination was about 87% in the visible range (400-650 nm) and 81% at the excitation wavelength (850 nm). For maximal transmission, we recommend using a coated offset lens to further optimize fluorescence collection efficiencies, because major transmission losses (~9%) for the complete spectrum (400-900 nm) were caused by reflections at our uncoated offset lens.

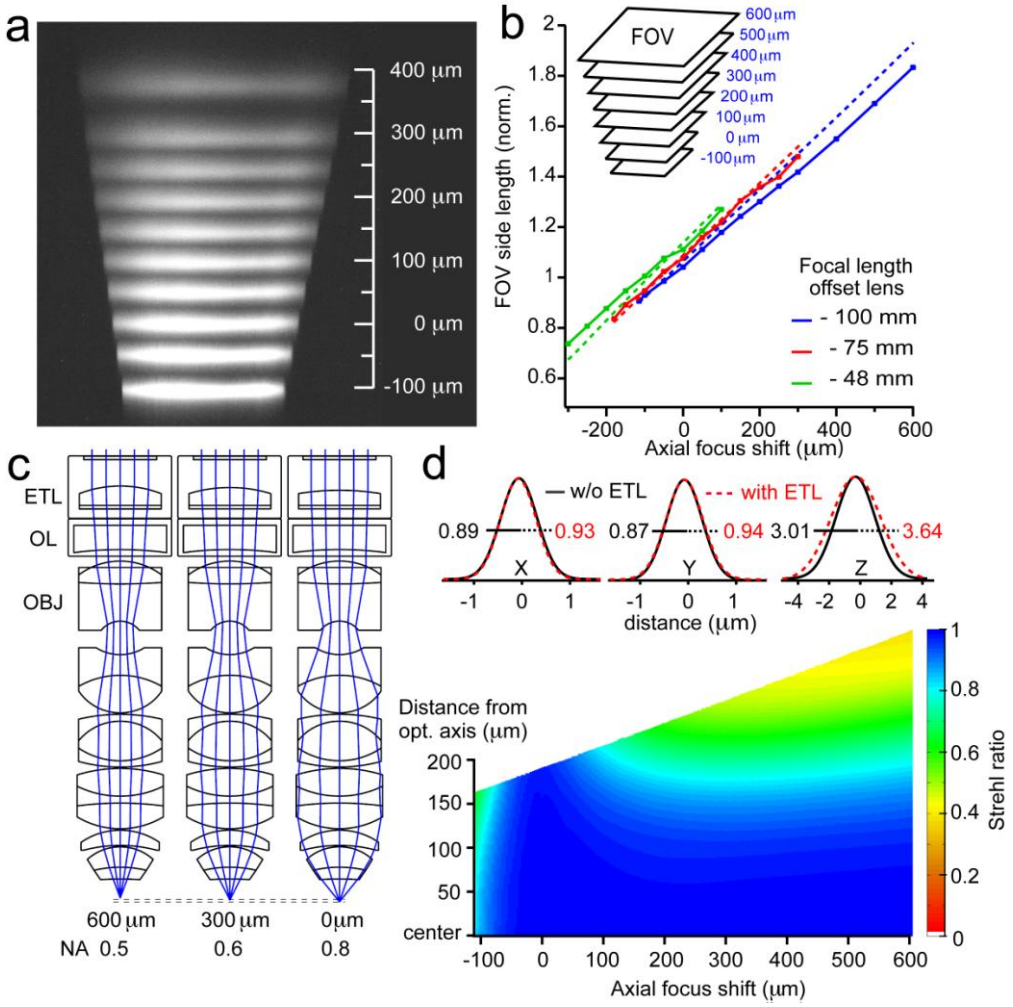

Fig. 2. Optical evaluation of the axial scanning method. (a) Side-view of the z-variations in FOV size visualized by line scans in a glass cuvette containing a Fluorescein solution. (b) Relative change of the field-of-view (FOV) size with axial focus shift with respect to the FOV size without ETL. The simulated change in FOV size is shown as dashed lines. (c) 2D ray tracing layout of the ETL/OL assembly with the microscope objective (OBJ) attached. The simulation was calculated for optimum filling of the ETL/Objective back aperture (BA). The change in NA with axial focus shift is apparent. (d) Upper panel: PSF measurements with and without the ETL/OL assembly at the zero z-position using a galvanometric scan mirror based two-photon microscope. All values are stated as PSF half-widths in µm. The fluorescent beads used were 500 nm in size (Fluoresbrite, Polysciences Inc.). Lower panel: Simulated Strehl ratios of the entire excitation path (with underfilled back aperture) at 850 nm as a function of distance to the optical axis and axial focus shift. Up to a distance of 200 µm from the optical axis, diffraction-limited performance can be maintained (Strehl ratio > 0.8).

#144186 - $15.00 USD Received 28 Mar 2011; revised 10 Jun 2011; accepted 10 Jun 2011; published 23 Jun 2011

2.3 Changes of the field-of-view size with axial focus position

By modulating the laser beam divergence we were able to induce precise axial shifts of the focal spot. Axial positions of the imaging plane were visualized by a side-view of subsequent line scans in a Fluorescein solution at different axial positions (Fig. 2a). As the position of the tunable lens assembly does not coincide with the (inaccessible) stop of the microscope objective, the system is, however, not telecentric. Thus chief rays of ray bundles directed at different sample points do not propagate in parallel to the optical axis after leaving the objective front lens, which results in a change of field-of-view (FOV) size with axial focus shift. Upon insertion of the ETL/OL combination in the microscope the FOV size slightly increased by 13.7% (−48 mm), 8.7% (−75 mm) or 6.5% (−100 mm) at the zero axial position (Fig. 2b; the zero position refers to the focus position without ETL/OL)

This offset is caused by the ETL/OL combination, acting as a Galilean telescope slightly compressing the beam diameter and thereby increasing the angular spread of the scanned beams entering the objective. When shifting the focus closer to the objective – thereby reducing the working distance – the FOV size increased linearly with a slope of about 13% per 100 µm (Fig. 2b). Using the optical design software ZEMAX (ZEMAX Development Corporation) we simulated the change in FOV size with axial focus shift, which was consistent with our experimental results (Fig. 2b, dashed lines).

2.4. Evaluation of optical performance

Every approach to defocus a standard microscope objective using optical means inevitably leads to a change of the numerical aperture (NA) accompanied by a shift of the axial focus position [23]. Assuming an optimal illumination of the ETL/Objective back aperture we simulated the resulting NA for the f = −100 mm offset lens at different axial positions, showing that with decreasing working distance, the NA decreases from 0.8 at z = 0 to 0.5 at z = 600 µm (Fig. 2c). However, using the AOD microscope we underfilled the ETL/Objective back aperture due to a trade-off between the FOV size necessary for population imaging and the limited scan angle of the AOD scanners [5]. Simulating the AOD microscope with the ETL/OL inserted we calculated the effective excitation NA ranging between 0.58 at z = −100 µm to 0.27 at z = 600 µm. At z = 0, an NA of 0.5 was obtained. To estimate the axial range and optical resolution properties of the ETL-microscope objective combination, we modeled the complete AOD microscope including a 40x objective using ZEMAX. Reasonable prescription data for the Olympus LUMPlanFL/IR 40x NA 0.8 was obtained from patent literature [24]; a ZEMAX model of the ETL was downloaded from www.optotune.com. Due to the diverging or converging beam at the rear stop of the objective, the careful balance of aberrations inside the objective is disturbed. When the focus is moved closer to the objective, thereby decreasing the working distance, the reduction of the NA and the resulting loss in resolution conceal the effects of newly introduced aberrations, allowing a large focus shift. When focusing down, however, the increase in NA leads to higher theoretical resolution and the aberrations become the limiting factor, thereby preventing diffraction-limited performance. In this case, only a small axial focus shift is possible before focusing-induced aberrations severely affect the optical performance.

To assess changes of the diffraction-limited single-photon PSF quality over the focusing range at an excitation wavelength of 850 nm, we simulated the Strehl ratio, which is defined as the ratio of the central peak intensities of the simulated PSF to an ideal diffraction limited PSF. This simulation revealed that diffraction-limited performance (Strehl ratio > 0.8) is possible for a FOV side length of 380 µm throughout axial shifts ranging from −70 to 600 µm with respect to the zero focus position (z = 0) (Fig. 2d). On the optical axis, a range of 700 µm is possible. The absolute values for lateral and axial resolution nonetheless changed considerably in this operating regime due to the variation of NA. Using a standard two-photon microscope with galvanometric scan mirrors we did not observe any significant changes in

#144186 - $15.00 USD Received 28 Mar 2011; revised 10 Jun 2011; accepted 10 Jun 2011; published 23 Jun 2011

resolution at z = 0 upon insertion of the ETL/OL assembly (Fig. 2d, upper panel) but the resolution decreased (particularly in axial direction) when focusing upwards with the ETL (Media 1). The observed changes in resolution are associated with the focusing-induced variation of the excitation NA. Similarly, with the AOD microscope, for which the resolution is limited by the AOD-scanners rather than by diffraction [5], we did not observe any decrease in resolution at the zero focal position (lateral ~0.8 µm, axial ~8 µm), while the resolution decreased when focusing upwards (Media 2). For most in vivo experiments, a smaller axial scanning range (from −100 to +200 µm) is sufficient, for which the axial and lateral resolution therefore may decrease by a factor of 1.5 and 1.7 for the galvo- and the AOD-based microscope, respectively. For both types of microscopes the imaging resolution is still sufficient to image neuronal cell populations within this smaller scanning range (Media 1 and 2).

2.5 Speed and reliability of ETL-based axial scanning

To measure the focusing speed of the ETL we built an "optical oscilloscope" that allows direct visualization of the focal spot z-position over time. By synchronizing AOD line scans with the driving signal of the ETL it was possible to generate repeated traces of the z-position over time, which, if viewed from the side in a fluorescent medium, resemble the visual impression of an oscilloscope signal.

A side view-microscope consisting of an air objective (Zeiss LD Achroplan 20x NA 0.4 Korr Ph2), a tube lens (f = 164 mm, Zeiss 425308), an IR rejection filter (ET 720SP, Chroma Technologies) and a CCD camera (pco.2000, pco AG), monitored the axial dynamics of the two-photon excited fluorescent focal spot within a Fluorescein solution at an angle of 90° with respect to the normal image plane (Fig. 3a). Using the correction collar of the side-viewing objective, the aberrations due to index mismatch between air, glass and the Fluorescein solution were minimized. Images were post-hoc registered using ImageJ [25] to yield z-t data not affected by non-uniformity in time caused by the variation of FOV size.

Registered optical oscilloscope traces were further analyzed using MATLAB (R2010b, Mathworks, USA) by fitting 2D Gaussian profiles along the vertical axis, to precisely evaluate the underlying axial position of the focal spot. To allow enough fluorescence light to be collected by the low-NA side-viewing microscope, many traces were averaged with a CCD exposure time of 8 s. This corresponds to 40 traces at 5 Hz and 6560 traces at 820 Hz for frequency/phase response measurements and 200 traces for step response measurements. We evaluated the amplitude and phase behavior of the ETL during oscillations of axial focal positions ranging from 1 to 820 Hz in steps of 5 Hz (Fig. 3c) controlled by a digital frequency synthesizer (AFG 3022, Tektronix) which was triggered using the microscope software. The resulting z-t traces were analyzed using a sinusoidal fitting routine in MATLAB to extract amplitude and phase (relative to the trigger signal). We found two maxima probably due to mechanical resonances at 310 Hz and 670 Hz, respectively, which are also reflected in the frequency response phase shift. To measure the step response times when switching between two imaging layers at different depths, we performed repeated line scans of 40 ms duration (n = 200, 8 s exposure time) while switching the ETL to preset axial focus positions (Fig. 3d). The registered z-t traces show fast initial oscillations of the ETL followed by a slow advance towards the preset axial position (Fig. 3e, red traces). To improve the time required to conduct axial focus displacements we modified the electric driving signal (Fig. 3e). We evaluated the time required to reach the set point by characterizing the decay of the oscillation by computing moving standard deviations in z over time. In a time window of 5 ms centered at 14.9 ±0.9 ms, the standard deviation settled below 1 µm for 20, 50 and 100 µm axial steps, which is low enough to start data acquisition on the new image plane. This analysis allowed us to set the switching time between two image planes to 15 ms which we used for the multi-layer imaging mode.

#144186 - $15.00 USD Received 28 Mar 2011; revised 10 Jun 2011; accepted 10 Jun 2011; published 23 Jun 2011

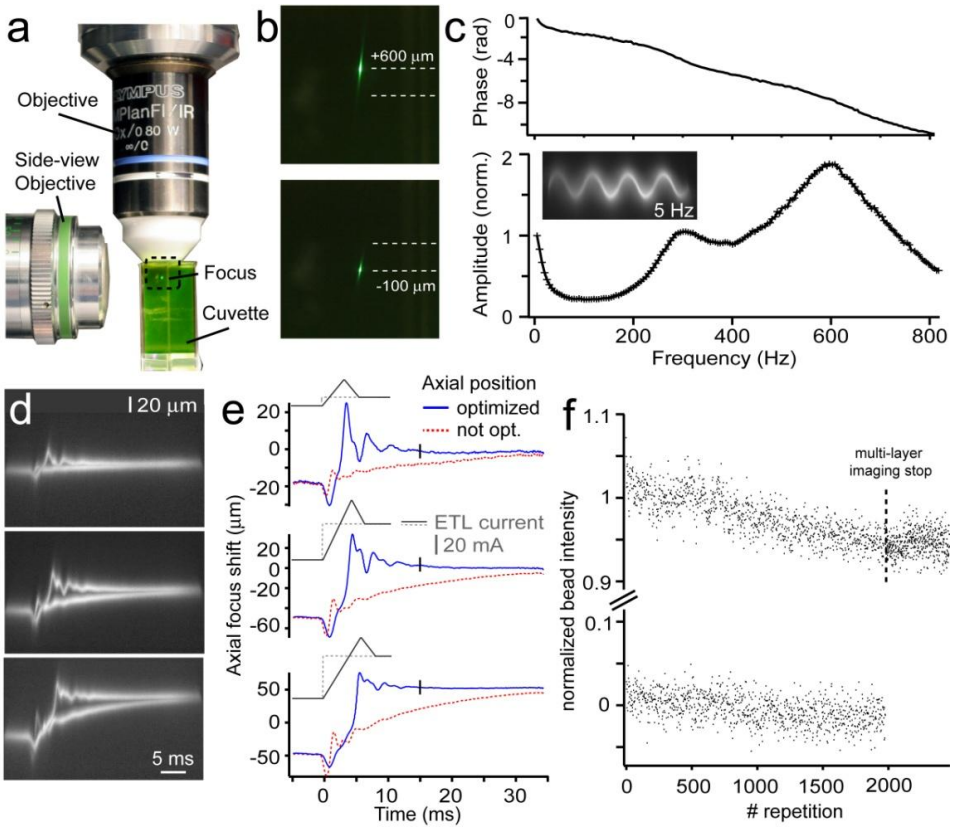

Fig. 3. Dynamical properties of the ETL. (a) Optical oscilloscope setup using a side-viewing microscope focused at the two-photon excited fluorescent spot in a cuvette containing a Fluorescein solution. (b) Magnified image as indicated in (a) shows the maximum axial focal shift of 700 µm using a f = −100 mm concave OL and the 40x objective. (c) Frequency-dependence of direct phase (upper panel) and amplitude normalized to the value at 1 Hz (lower panel) of the ETL/OL/Objective axial scanning system in response to a sinusoidal driving current. Two broad resonance peaks at 300 and 600 Hz are discernible (5 Hz step size). Traces recorded with an eight second exposure time; according to the applied sinusoidal driving signals (5-820 Hz) 40-6560 traces were averaged. Example image shows a typical trace recorded for 5 Hz ETL oscillation frequency. (d) Optical oscilloscope traces showing step response and response using an optimized driving signal. In each case 200 traces were recorded. (e) Registered optical oscilloscope traces after image processing showing the step response with and without optimizing the ETL-current driving signal (gray traces on top of the reconstructed step responses) for different axial steps around the focus position without ETL/OL (z = 0). Employing optimized driving signals axial target positions were reached after 15 ms (indicated by black ticks). (f) Measurements of normalized bead intensities using the AOD frame scanning (5 Hz frame rate) at two different focal depths (step size 35 µm) during 2000 repetitions. Note: Beads were in focus only when switching to the upper axial layer. The position accuracy of axial positioning was then derived offline by a deconvolution of the normalized bead intensity (measured at the center of the bead) with the z-resolution of the AOD microscope (7.9 µm). Our analysis revealed an axial accuracy below 1 µm (±0.42 µm).

To assess whether the axial pointing repeatability is sufficient for extended in vivo imaging sessions, we evaluated the bead intensity of 1 µm fluorescent beads during repeated switching between two imaging layers. To determine the precise axial focal position the measured bead intensities (at the center of the bead) were normalized and assigned to the axial resolution function of our AOD microscope (7.9 µm, using 1 µm beads). During 2000 repeated switching cycles at a frame rate of 5 Hz, bead intensities showed a small decrease to about 95%, probably due to a slight temperature drift of the ETL (Fig. 3f, step size 24 µm).

#144186 - $15.00 USD Received 28 Mar 2011; revised 10 Jun 2011; accepted 10 Jun 2011; published 23 Jun 2011

However, our analysis revealed that within this operating regime, the axial position accuracy of the ETL is still below 1 µm (±0.77 µm, n = 3 beads, z-step of 35 µm).

The ETL in combination with the f = −100 mm offset lens and the optimized driving signal thus allows fast, reliable axial shifting of the focal spot to image different optical planes along the optical axes, as shown in Media 3, depicting rapid switching between two layers while scanning a group of pollen grains.

3. Two-layer in vivo calcium imaging of neuronal population activity

With a suitable minimal step response time of 15 ms we next tested the ETL in combination with the 2D AOD microscope for in vivo two-photon imaging to record spiking activity of neuronal cell populations. Cell populations in layer 2/3 of mouse barrel cortex were bolus-loaded with the calcium indicator Oregon Green BAPTA-1 (OGB-1) [26]. In some experiments, astrocytes were additionally labeled by brief application of sulforhodamine 101 (SR101) to the cortical surface [27]. Animal surgery, cranial window preparation and cell labeling was performed as previously described [5]. All animal procedures were carried out according to the guidelines of the Center for Laboratory Animals of the University of Zurich and were approved by the Cantonal Veterinary Office.

Focusing with the ETL allowed imaging throughout a large volume of stained tissue as visualized by an in vivo recorded z-stack through the cortex (Fig. 4a and Media 4). Setting the zero focus position to a depth of about 200 µm (below the pia mater) the ETL permits fast focusing from the cortical surface down to about a depth of about 300 µm, mostly limited by the extent of the stained volume and the maximal two-photon penetration depth suitable for functional imaging. Using an axial focusing range of about −100 µm to + 200 µm during in vivo experiments we did not observe any noticeable effect of ETL focusing on functional measurements of neuronal population activity that can be traced back to the accompanying changes of the FOV size and the imaging resolution (Media 1, 2 and 5).

For functional 3D imaging, we combined repeated axial shifting of the focal spot either with 2D frame imaging or high-speed random access pattern scanning (RAPS) [5] employing the AOD scanner based microscope (Fig. 4b). First, we used AOD frame scanning, to record alternating images of neuronal cell populations in L2/3 at two different depths during sensory stimulation of the barrel cortex by short, 20-30 ms air puffs to the contralateral whiskers. With a maximum frame scan rate of 6 Hz we were able to obtain population activity signals from OGB-1 loaded L2/3 neurons with an imaging rate of 3 Hz per layer (Fig. 4c). To further improve the scanning speed we used high-speed acousto-optic random-access-scanning and combined the RAPS mode with fast axial ETL focusing. In RAPS mode, each cell is subject to a sub-pattern scan of several points to improve fluorescence signal acquisition at high-speed sampling rates while maintaining a sufficient SNR. In our case we preselected 17 neuronal somata (plus 3 background regions) in each imaging plane from two reference images. RAPS imaging was performed using a 9-point pattern and a total signal integration time of 80 µs per cell (+ 10 µs cell-to-cell transition time). For the experiments shown in Fig. 4d we used a switching time of 21 ms. In general, the total sampling rate f_{tot}, for n layers, is given by

$$f_{\mathrm{tot}} = \frac{1}{\sum_{k=1}^{n}\left(\tau_{\mathrm{acq},k} + \tau_{\mathrm{switch}}\right)}, \qquad (1)$$

where $t_{ack,k}$ is the imaging time to image all selected cells within layer k, and t_{switch} is the switching time of the ETL. Given the total integration time of 3.6 ms for 40 locations plus 2*21 ms for ETL switching, we were able to record neuronal population activity signals of 40 spots (20 for each layer) with a rate of 21.6 Hz (Fig. 4d). In several additional experiments we also used 15 ms ETL switching time resulting in a 30-Hz effective acquisition rate. We

#144186 - $15.00 USD Received 28 Mar 2011; revised 10 Jun 2011; accepted 10 Jun 2011; published 23 Jun 2011

conclude that AOD-RAPS in combination with an ETL as fast axial scanner allows video-rate monitoring of neuronal activity signals across multiple planes in 3D.

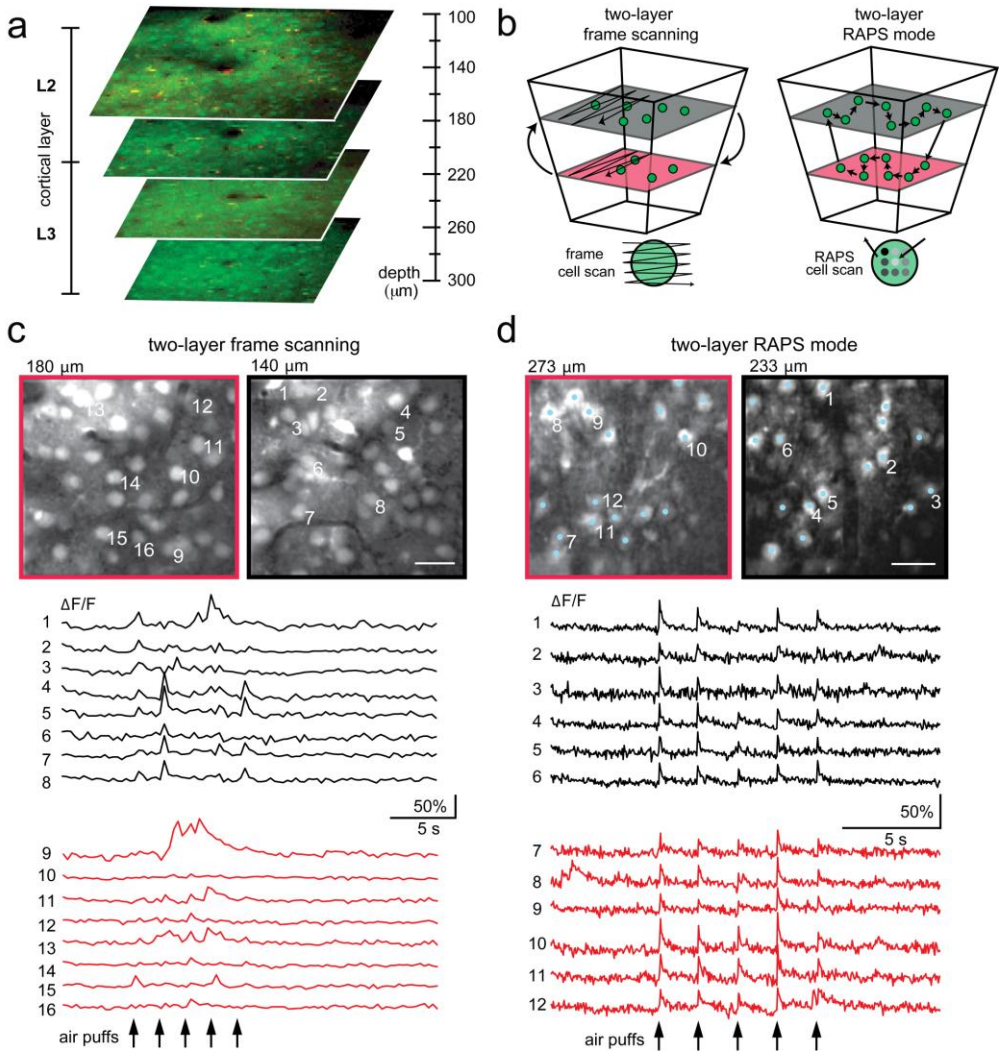

Fig. 4. Two-photon two-layer calcium imaging in mouse neocortex. (a) Two-photon images of a neuronal cell population (green) stained with OGB-1 in L2/3 throughout mouse neocortex starting at 100 μm below the pia. (b) Schematic drawing of two-layer frame scanning and two-layer random-access pattern scanning at different depths. (c) Upper panels: Two L2/3 neuronal cell populations (gray) labeled with OGB-1-AM in mouse barrel cortex. Calcium imaging of neuronal cell populations was performed at different depths below pia mater (left image 180 μm, right image 140 μm). Scale bar, 20 μm. Lower panel: Neuronal activity signals (expressed as relative percentage fluorescence changes ΔF/F) were recorded at 6-Hz frame scanning rate (3 Hz per plane). To induce neuronal activity repeated brief air-puffs were applied to the mouse contralateral whiskers (indicated by black arrows). (d) Upper panels: Two-photon images of a neuronal cell population (gray) stained with OGB-1. Images are recorded at different focal depths (left image 273 μm, right image 233 μm) in mouse barrel cortex. The preselected random-access scanning positions on neuronal somata are shown as blue dots. Scale bar, 20 μm. Lower panel: Fast two-layer imaging was performed using 9-point RAPS targeted to 40 spots (17 cells for each layer plus background spots) that were manually pre-selected from the two reference images. Relative fluorescence traces (ΔF/F, 12 example cells shown) were recorded during short air-puff stimulations of the contralateral whiskers (black arrows). Effective sampling rate was 21.6 Hz. In vivo imaging experiments in (c) and (d) were performed using the 100 mm offset lens.

#144186 - $15.00 USD Received 28 Mar 2011; revised 10 Jun 2011; accepted 10 Jun 2011; published 23 Jun 2011

4. Discussion

By combining the ETL as a fast axial scanning device with high-speed AOD-RAPS imaging, we demonstrated a versatile and expandable method for fast three-dimensional in vivo population imaging of neural networks. A major advantage of using ETLs as z-scanners is that they offer a relatively large aperture while maintaining fast focusing response times—in our case about 15 ms switching time was achieved. To avoid severe distortion of the excitation wave front apart from the deformation necessary for axial scanning we chose a combination of ETL, OL and microscope objective, which ensures sufficient optical performance over a considerably large axial focusing range. Because focusing speed and aperture size usually correlate inversely, standard liquid variable-focus lenses that are based on electrowetting are, however, not fast enough for such applications or they are only available with relatively small aperture sizes [17,18]. Nevertheless, fast focusing has been demonstrated with custom built hydraulic tunable lenses with larger aperture sizes, but it is not clear whether such lenses provide a sufficient focusing accuracy over thousands of repetitions [16].

The ETL we used offers fast axial scanning in combination with a large aperture and allows accurate focusing for in vivo imaging over thousands of repetitions. ETLs are commercially available, inexpensive and can be easily added to any two-photon microscope. The non-telecentric use of the ETL/OL lens assembly directly before the objective leads to a change in the FOV size. If necessary, this effect could be avoided by placing the ETL and OL at the original position of the objective and using an additional 4f-system composed of two achromats to reimage the pupil onto the relocated microscope objective, rendering the optical system telecentric at $z = 0$. In particular, this might facilitate imaging studies that are based on precise morphological reconstruction, where a constant magnification with axial focus shift might be necessary. Another advantage is that in this configuration, the emitted light would not pass the ETL/OL assembly as it is reflected onto the fluorescence detectors by a dichroic mirror placed close to the objective, which will improve the fluorescence light detection efficiency. For functional calcium imaging of neuronal networks a change in the FOV size does not significantly influence the measurements as long as the focal z-position can be reproduced accurately. The AOD microscope we employed is optimized for fast 2D random-access scanning of neuronal cell populations, as such, its functionality is not being affected by the variation of the FOV. Using a piezo-electric focusing element to perform 3D line scanning previous approaches have demonstrated in vivo imaging of large cell populations with a 3D sampling rate of up to 10 Hz [4]. While this approach was mostly limited by the scanning speed of the axial scanner, due to the weight of the objective, it can be extended to higher sampling rates by using an ETL as z-scanning device.

Alternatively, fast multi-layer imaging can be achieved with spatiotemporal multiplexing techniques [15,28], which focus temporally separated laser pulses at different depths while using the timing of the detected fluorescence to assign the signal to the correct imaging plane and pixel position. However, reported implementations rely on galvanometric frame-scanning, which restricts their temporal resolution to about 20-30 Hz to achieve sufficient SNR for measuring population activity. Nonetheless, such techniques might benefit from incorporation of ETLs as well, because ETLs would enable fast axial positioning of a number of arbitrary image planes of interest within a 3D volume. Other promising approaches for rapid 3D population imaging may include remote focusing schemes [9,10] and random-access imaging systems utilizing multiple AODs [12,13], albeit at much higher technical complexity. In this study our aim was to design a relatively simple axial scanning method well suited for upgrading existing two-photon microscopes with fast 3D scanning capabilities. All main optical components such as the ETL and the offset lens are readily available and beam path alignment is very simple with only three key adjustable components (ETL/OL/Objective).

In summary, we have implemented a simple and effective way to access the third dimension for fast functional in vivo two-photon microscopy of neuronal populations. Further

#144186 - $15.00 USD Received 28 Mar 2011; revised 10 Jun 2011; accepted 10 Jun 2011; published 23 Jun 2011

improvements in the technology of electrically tunable lenses will most likely allow much higher volumetric imaging rates, since ETLs with faster step response times will be available in the near future [29]. Furthermore, our approach can be considered as an option to transform different microscope types such as confocal laser scanning microscopes or standard wide field microscopes into fast 3D imaging platforms, which renders this technique attractive not only for microscopists and neuroscientists but also for the larger biological and biomedical research community.

Acknowledgments

We thank Mark Blum (Optotune AG) for providing various ETLs and for fruitful discussions. We thank David Margolis for comments on the manuscript and we are grateful to Stephan Giger for mechanical work and to Hansjörg Kasper and Martin Wieckhorst for technical assistance. Also we would like to thank Morgane Roth for helping with the in vivo experiments. This work was supported by a Forschungskredit of the University of Zurich (B.F.G.), and by grants to F.H. from the Swiss National Science Foundation (Grant 3100A0-114624), the EU-FP7 program (Brain-i-nets FP7-2009-ICT-FET 243914), and the Swiss SystemsX.ch initiative (project 2008/2011-Neurochoice).

#144186 - $15.00 USD Received 28 Mar 2011; revised 10 Jun 2011; accepted 10 Jun 2011; published 23 Jun 2011